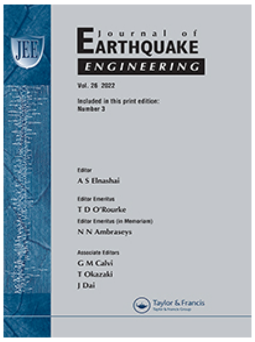

Taylor & Francis
Taylor & Francis Group

Journal of Earthquake Engineering

ISSN: (Print) (Online) Journal homepage: https://www.tandfonline.com/loi/ueqe20

Experimental Seismic Performance of Partly-Sliding Partition Walls

J. Mulligan, T. J. Sullivan & R. P. Dhakal

To cite this article: J. Mulligan, T. J. Sullivan & R. P. Dhakal (2022) Experimental Seismic Performance of Partly-Sliding Partition Walls, Journal of Earthquake Engineering, 26:3, 1630-1655, DOI: 10.1080/13632469.2020.1733139

To link to this article: https://doi.org/10.1080/13632469.2020.1733139

Published online: 09 Mar 2020.

JOURNAL OF EARTHQUAKE ENGINEERING
2022, VOL. 26, NO. 3, 1630–1655
https://doi.org/10.1080/13632469.2020.1733139

Taylor & Francis
Taylor & Francis Group

Experimental Seismic Performance of Partly-Sliding Partition Walls

J. Mulligan, T. J. Sullivan, and R. P. Dhakal

Department of Civil and Natural Resource Engineering, University of Canterbury, Christchurch, New Zealand

ABSTRACT

Plasterboard partition walls typically used in commercial buildings are especially sensitive to earthquakes, with the onset of cosmetic damage initiating at small values of interstorey drift. The most common partition wall systems are constructed of gypsum board attached to either steel or timber framing which is fixed directly to the floor system at the top and bottom interfaces. This study investigates the seismic performance of a novel partly-sliding steel-framed partition system examined in the past and used by industry, with minor modifications incorporated within the partition detailing. This novel system involves removing top track anchors within the proximity of wall intersections, thus allowing the tracks to 'bow' out at these locations. In this study three full-scale specimens were subjected to quasi-static cyclic testing; two identical plane specimens and the third including a doorway. The specimens were built in a y-shape and angled at 30° to the direction of applied loading, which allowed bi-direction behaviour to be examined. The specimens included an acoustic/fire sealant. The progression of damage in a partition can be categorized by three sequential damage states associated with distinct levels of repair: superficial damage requiring cosmetic repair (damage state 1 (DS1)), damage requiring local repairs or replacement of only portions of the partition assembly (damage state 2 (DS2)), and severe damage requiring complete removal and replacement of the wall (damage state 3 (DS3)). Damage was first observed as cracking of the wallboard at the wall ends, at external junctions, and propagating from the corners of the door opening. The onset of DS1 and DS2 occurred simultaneously at a median in-plane drift of 0.29%. DS3 was not observable until the linings had been removed at the end of the tests. In addition to providing drift capacities, the force-displacement behaviour is also reported, the dissipated energy was computed, and the parameters of the Wayne–Stewart hysteretic model were fitted to the results. The specimen with the door opening behaved significantly different to the plane specimens: damage to the doorway specimen began as cracking of the wallboard propagating from the corners of the doorway following which the L- and Y-shaped junctions behaved independently, whereas damage to the plane specimens began as cracking of the wallboard at the top of the L-junction and wall system deformed as a single unit. The results suggest that bi-directional behaviour is important even if its impact cannot be directly quantified by this experiment. Damage to sealant implies that the bond between plasterboard and sealant is important for its seismic performance, and careful quality control is advised, as defects in the bond may significantly impact its ability to withstand seismic movement.

ARTICLE HISTORY
Received 6 June 2019
Accepted 18 February 2020

KEYWORDS
Plasterboard partition walls; fragility curves; non-structural elements; drywall; acoustic/fire sealant

CONTACT T. J. Sullivan timothy.sullivan@canterbury.ac.nz Department of Civil and Natural Resource Engineering, University of Canterbury, Private Bag 4800, Christchurch 8140, Christchurch, New Zealand

1. Introduction

It is now widely recognized that the performance of non-structural elements is a crucial component of the performance of building systems during earthquakes (Dhakal 2010). Their performance is vital to maintain continuity of emergency and recovery services, to reduce the likelihood of injury or death, to prevent loss of building function, and to limit the direct and indirect economic losses resulting from earthquake events. Taghavi and Miranda (2003) have shown that non-structural elements comprise the majority of investment in commercial buildings (Fig. 1). Furthermore, for all building types, interior construction was shown to comprise 20–30% proportion of the non-structural component cost. Partition walls, also known as drywalls, have been shown to significantly contribute to total earthquake losses. Whitman, Hong, and Reed (1973) found that in the 1971 San Fernando Earthquake, for buildings in earthquake intensity (MMI) zones VI, VII, and VIII, the damage to partitions contributed approximately 90%, 65%, and 50% respectively, to the total cost of damage to buildings. They concluded that improving the seismic performance of interior partitions would be one of the most effective ways to reduce the seismic losses in buildings subjected to MMI VI earthquakes. This is because partition walls are especially sensitive to earthquake damage, with the onset of damage initiating at low interstorey drifts of approximately 0.35% according to Davies et al. (2011). This level of interstorey drift may be imposed by low-intensity ground motions with frequent return periods and this implies frequent repairs after relatively small earthquake events or aftershocks, resulting in significant financial loss (Arifin et al. 2017).

Performance-based earthquake engineering (PBEE), described in the FEMA P58 document (FEMA 2012), provides a framework by which buildings can be designed using performance objectives that are system level in terms of risk of collapse, fatalities, repair costs, and post-earthquake loss of function. In order to provide a rigorous probabilistic assessment of losses, PBEE utilises fragility and loss functions. Fragility functions can provide a probabilistic means of quantifying the likely level of damage in a component given a particular structural response. The levels of damage are expressed as damage states corresponding to a level of repair and the structural response is quantified by a particular engineering design parameter (EDP) that correlates well with damage. For light framed

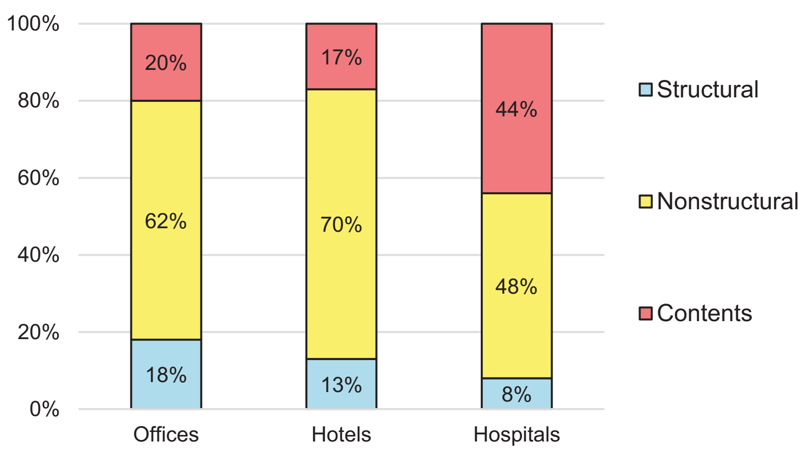

Figure 1. Building construction cost distribution of components of three sample buildings as a percentage of total cost (Taghavi and Miranda 2003).

steel or timber plasterboard partition walls, damage states have shown to correlate best with in-plane interstorey drift (Freeman 1971; Rihal 1980; Taghavi and Miranda 2003).

The earliest experimental investigations on gypsum lined walls were focused on the load-deformation of shear walls designed to resist lateral loads (Deierlein, Krawinkler, and Allin Cornell 2003). The earliest series of tests that the author is aware of on commercial non-structural partition walls was conducted by Lee et al. (2007). Lee et al. (2007) tested full-scale partitions with lightweight steel framing according to typical Japanese configurations and estimated a damage-repair cost relationship. Overall, the specimens were damage free until up to 0.25% interstorey drift.

Restrepo and Bersofsky (2011) tested 2.4 m high 2.9 m long I-shape partition wall specimens with 1.2 m returns at each end, under quasi-static reversed cyclic displacement based on in-plane loading according to the CUREE loading protocol for wood-frame structures (Krawinkler et al. 2001). Restrepo and Bersofsky (2011) used the damage state (DS) definition recommended by Taghavi and Miranda (2003) for drywall wood stud partition walls: (1) cracking in plaster and paint, (2) damaged drywall panel, and (3) damage to framing. For conventional steel stud partitions DS1, DS2, and DS3 occurred at drifts of 0.3%, 1%, and 3%, respectively.

The most extensive series of experiments into the seismic performance of plasterboard partition walls appears to have been conducted by Davies et al. (2011). The authors tested 50 full-scale partition walls in 22 different configurations under both quasi-static and dynamic loading and generated data regarding the in- and out-of-plane seismic behaviour. Variables included return wall configurations; partial-height and full-height specimens; alternate junction details; connectivity of studs, tracks, and sheathing; and bookshelf attachments. This data was used to produce a set of fragility parameters, useful for implementation in PBEE analysis of buildings. For the development of the fragility parameters, the authors used damage states previously defined by Taghavi and Miranda (2003). The typical test specimens were 3.5 m high by 3.7 m long. For the test specimens close to NZ commercial partitions, the mean drifts associated with DS1, DS2, and DS3 were 0.26%, 0.68%, and 0.75%, respectively. It should be noted that DS3 was triggered at a relatively low drift. This was failure of the track to concrete fasteners at the ends of return walls. The track to concrete fasteners used by were standard powder driven 25 mm (1″) fasteners @ 610 mm (24″) centres, using a Ramset gun model SA-270 and Ramset.27 caliber shots. Similar fasteners were used by Restrepo and Bersofsky (2011) at a larger spacing (812 mm centres) driven in by a 0.22 caliber nail gun-plus. However, this form of damage was not observed as additional fasteners were placed at the end of return walls.

Included within the series of tests by Davies et al. (2011) were some novel details for improving the performance of partitions, including a ‘sacrificial corner bead’ system (specimen 33 & 35), and a flexible track system (specimen 34 & 36). Other systems have been proposed in the literature for the improvement of the seismic performance of partitions: including a sliding/frictional system developed by Araya-Letelier and Miranda (2012), and a gapped system tested in several studies (Lee et al. 2007; Magliulo et al. 2014; Pali et al. 2017, 2018; Tasligedik, Pampanin, and Palermo 2015).

The flexible track system proposed by Davies et al. (2011) is the focus of this study. Retamales et al. (2013) suggested that ‘practical considerations of the new proposed details would require evaluation of other design constraints including bidirectional seismic loading, acoustic transmission, and fire resistance’ and that ‘additional tests are required to evaluate their effectiveness’. Through conversation with the industry, it appears that a partially-sliding partition wall system with similar detailing to that tested by Davies et al. (2011) is used in practice. As such, this work reports an experimental campaign that tests partially sliding partition walls in order to investigate the effect of bi-directional behaviour, angled return walls, and door openings; and to develop fragility functions. The tests aim to investigate the seismic behaviour of fire/acoustic sealant when used in practice at the top lining to floor boundary.

2. Details of Partially Sliding Partition Walls

In New Zealand, steel-framed drywalls are typically constructed of light gauge steel studs sheathed with gypsum wallboard (GIB) screwed to the framing. There are various alternatives in connections and configurations including, steel framing size and gauge; fastener type, spacing, and location; sheathing type, orientation, and number of layers; top and bottom track anchors; and others. Guidelines are available that recommend different configurations depending on various performance objectives including, fire rating, sound rating, impact resistance, and other special purposes. The configuration chosen to provide a baseline for this experimental study was a fire-rated partition typology selected from GIB Fire Rated Systems (GIB 2012), with a 60-min fire-resistance rating (GBS60). The steel framing consisted of $92 \times 34 \times 0.5$ studs $94 \times 30 \times 0.5$ base tracks provided by RONDO. The framing was sheathed with 13 mm GIB Fyreline®, connected with 25 mm × 6 g GIB Drywall Self Tapping Screws® at 300 mm centres up each stud with an additional screw between the lining and bottom track between each stud. Bottom and top track anchors were HILTI HUS3-H8 × 55 screw anchors at 600 mm centres.

The flexible track system proposed by Davies et al. (2011) increases track flexibility by not using track to concrete slab connectors within 610 mm (2′) of wall intersections, thus allowing the tracks to 'bow' out. Davies et al. (2011) proposed two specimen designs. For the first specimen, only the top track anchors were removed, the studs and plasterboard were screwed to the bottom track, and the studs were free to slide within the top track. For the second specimen, both top and bottom anchors were removed in proximity to junctions, and the studs and linings were not connected to the track at the top or bottom, and so were free to slide at both ends.

The specimen design for this test series, termed "partially-sliding", was developed considering the designs by Davies et al. (2011) and in discussion with an industry partner who has been producing a similar system. The design incorporates only minor alterations to the as-built NZ GBS 60 partition wall. The changes are to remove top track fixings within the proximity of return walls and to fix the sheathing to the bottom track at 600 mm centres, but not at the top; the objective of this being that the studs are free to slide within the top track while the sheathing remains stationary. The junction details were developed in consultation with industry. The return walls were approximately 600 mm long and were configured in a 'y' shape, with two return walls at a 90° angle to the main wall and one at 45°, as shown in Figs. 2 and 3. This configuration was chosen as no previous studies the author is aware of had considered the impact of oblique walls. In addition, a 25 mm gap at the top of the sheathing was provided and filled with fire sealant, as is common in practice, with tape along the track flanges in order to break the bond between top track and sealant (Fig. 4). The fire sealant used for this application was HILTI CP606 flexible fire stop sealant. The main difference between this specimen design and the specimens tested by Davies et al. (2011) was the junction details. Davies et al. (2011) tested an I-shaped specimen with two

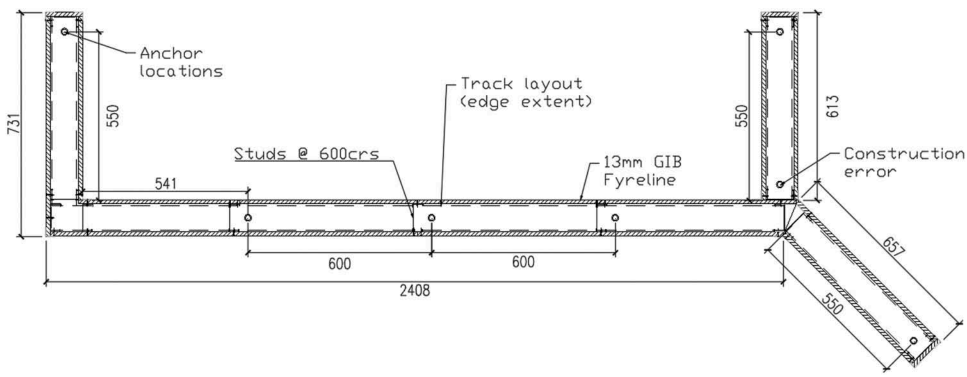

Figure 2. Specimen A1&A2 dimensions with top track anchor locations (dimensions in mm).

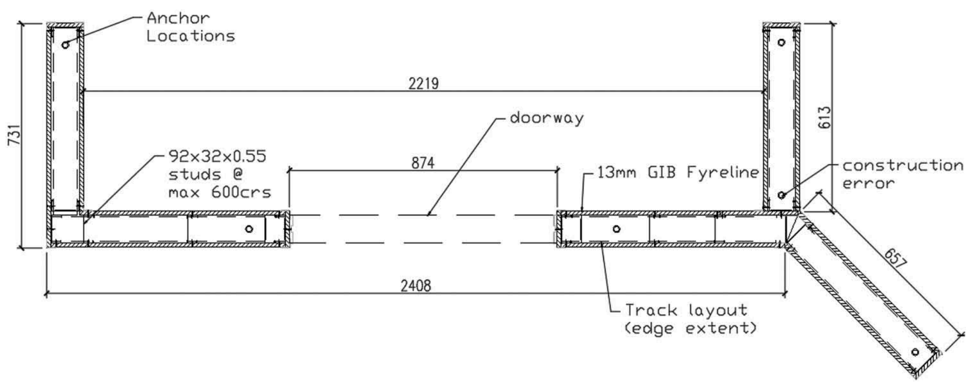

Figure 3. Specimen A3 plan dimensions and top track anchor locations (dimensions in mm).

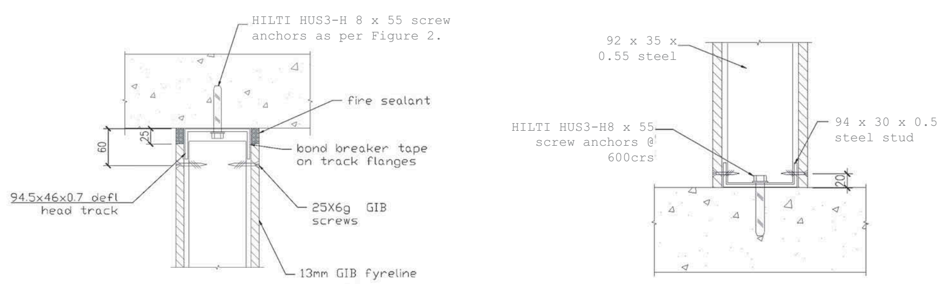

(a) (b)

Figure 4. (a) Top slab connection, (b) base slab connection.

T-shaped junctions, whereas the specimens studied herein were in a y-shape with one L-junction and one Y-junction. Some other differences from the specimens tested by Davies et al. (2011) were that the studs were not fixed to the tracks at any location; and more robust track anchors were utilised to avoid the early anchor failure experienced in both of their tests.

Although the top track anchors were specified to be removed within 600 mm of wall intersections, a construction error was made whereby a single top track slab to concrete anchor was left in at the three-way wall junction (Fig. 4). The potential impact of this error is discussed when reviewing results. Despite this error, the experimental testing was deemed worthwhile since such errors will also occur in practice and because the behaviour of the wall can be examined with this fixing in mind.

3. Experimental Test Setup

3.1. *Testing Frame*

The walls were tested in racking in order to simulate the loading experienced by partition walls in commercial buildings. The testing frame was hinged at the top and the bottom in-plane, with diagonal braces to provide stability while the actuator is not attached. The frames are constructed of steel 125PFC members. The top and bottom concrete boundaries are 120 mm thick-reinforced concrete slabs, which were selected in order to simulate the most typical boundary conditions and flooring systems in real buildings. The plan dimensions of compartment including the partitions were 3175 mm by 2100 mm, and the clear height was 2405 mm (Fig. 5a,b). Three separate frames were constructed, in order to allow swift construction and testing (Fig. 5c,d). The response of the bare frame was approximately linear with a stiffness of 10.1 N/mm, as shown in Fig. 6.

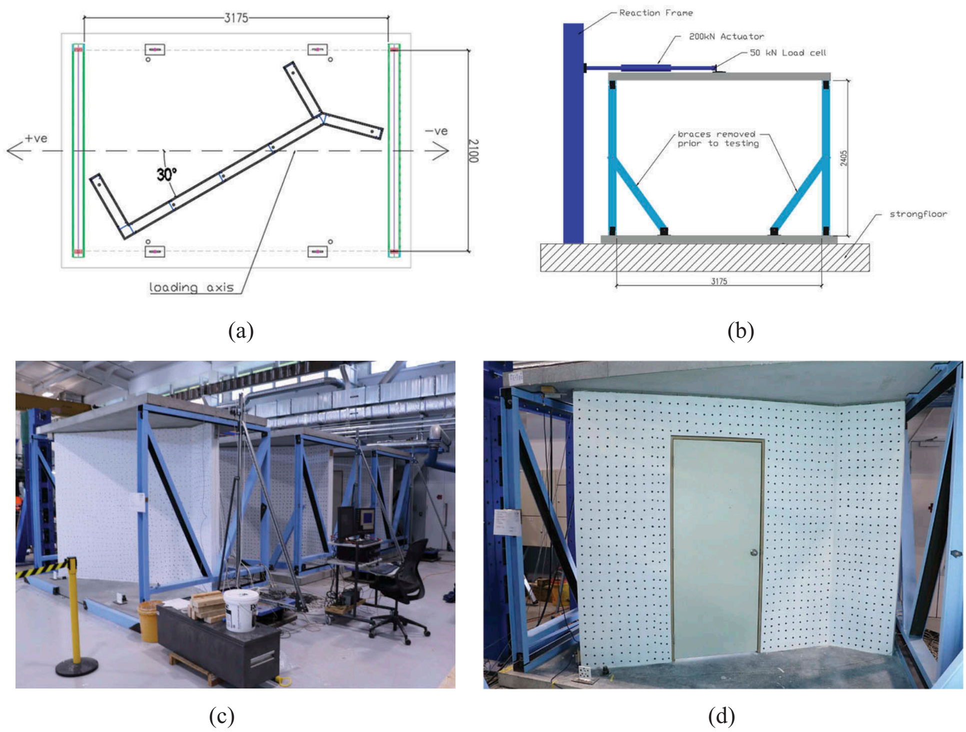

Figure 5. (a) Plan of testing frame (mm); (b) Elevation of testing frame (mm); (c) Photograph of setup; (d) Photograph of specimen A3 (doorway specimen).

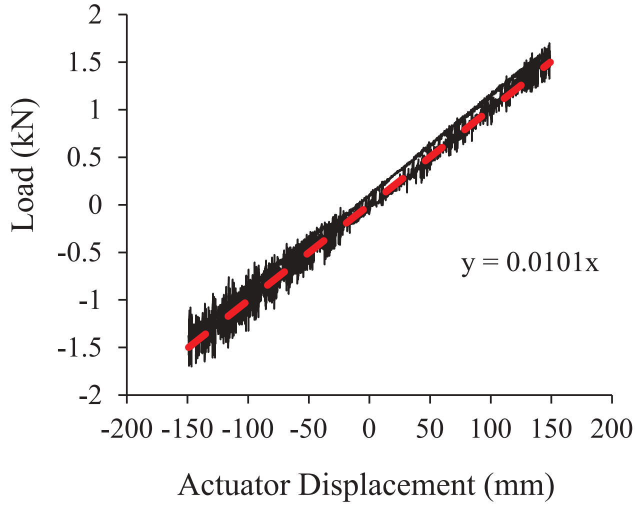

Figure 6. Load displacement behaviour of the bare frame.

3.2. *Experimental Program*

Three partition-wall specimens were tested in this experiment: two (A1 & A2) identical to those shown in Fig. 2, and a third specimen, A3, that was also identical except that it possessed a door (see Fig. 3). To assess the impact of bidirectional loading on fragility, the wall specimens were aligned at an angle of 30° to the loading direction, as shown in Fig. 5a. The specimens were tested according to FEMA 461 deformation-controlled unidirectional quasi-static cyclic protocol (FEMA 2007). The protocol was calibrated based on the results of previous in-plane tests on similarly detailed walls (Restrepo and Bersofsky 2011). The estimated drift for DS1 was 0.3% and the target maximum drift was 5%. Two cycles were applied at each drift amplitude and the drift amplitude of each step was 1.4 times the amplitude of the preceding step. A total of 16 drift steps were applied, up to a maximum drift of 6.21% (Fig. 7), which corresponds to a maximum in-plane drift of 5.38% for the wall angled at 30°. Specimens A1 & A2 were tested up to step 15 and specimen A3 was tested up to step 16.

3.3. *Data Acquisition*

The load applied to the specimens was recorded with a 50 kN load cell with an accuracy of ±3 N. The specimens were instrumented with a combination of linear potentiometers and cameras. With reference locations shown in Fig. 8, the general potentiometer layout for the test series is shown in Fig. 9. For the first specimen, 30 potentiometers were used to measure the horizontal, vertical, and lateral deflections; however, the number of potentiometers was reduced to 23 by the third specimen as some of the instruments were deemed unnecessary. The potentiometers recorded the linear relative displacement between the location they were fixed on the wall and the surface of the concrete slab closest to their location. The cameras were used to record frames at each displacement increment in order to enable particle tracking software analysis. A series of high contrast points at approximately 75 mm spacing were applied to the surface of the specimens for this purpose.

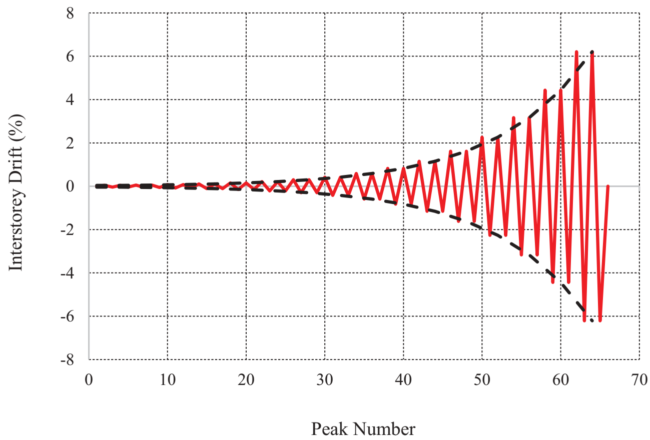

Step	Top Slab Disp (mm)	Drift (%)
1	0.96	0.04
2	1.3	0.06
3	1.9	0.08
4	2.6	0.11
5	3.7	0.15
6	5.2	0.21
7	7.2	0.3
8	10.1	0.42
9	14.2	0.59
10	19.8	0.82
11	27.8	1.15
12	38.9	1.62
13	54.4	2.26
14	76.2	3.17
15	106.7	4.44
16	149.3	6.21

Figure 7. FEMA 461 quasi-static cyclic displacement protocol.

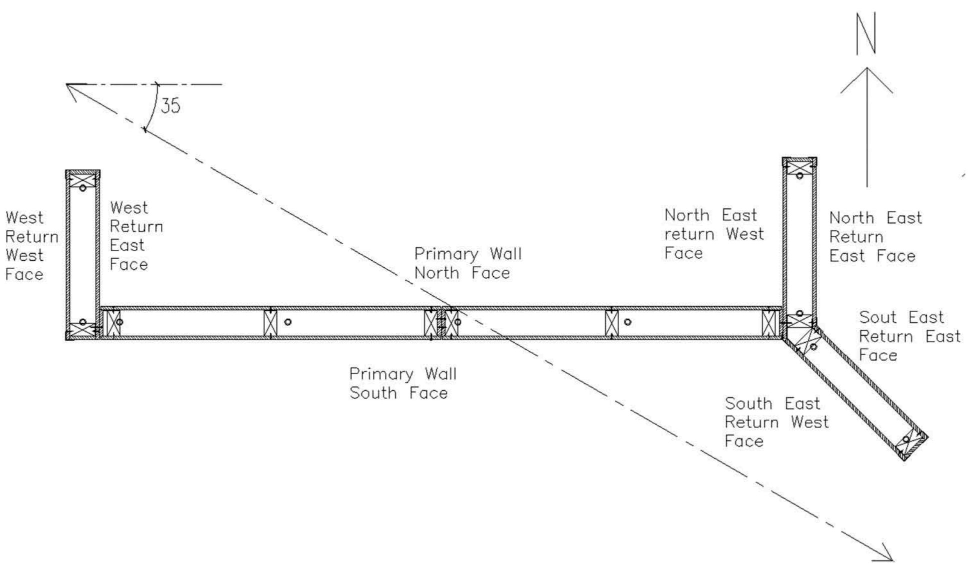

Figure 8. Wall specimen showing references for wall locations.

4. Results

4.1. *Damage Observations*

Damage observations were taken after each step in the loading protocol (Fig. 7), these included detailed visual inspections and photographs. As only visual observations were made, the point at which the framing was damaged could not be identified until the wall-board began to spall, which happened only in the doorway specimen. Thus, only at the completion of the test could a detailed inspection of the framing be made. The forms of

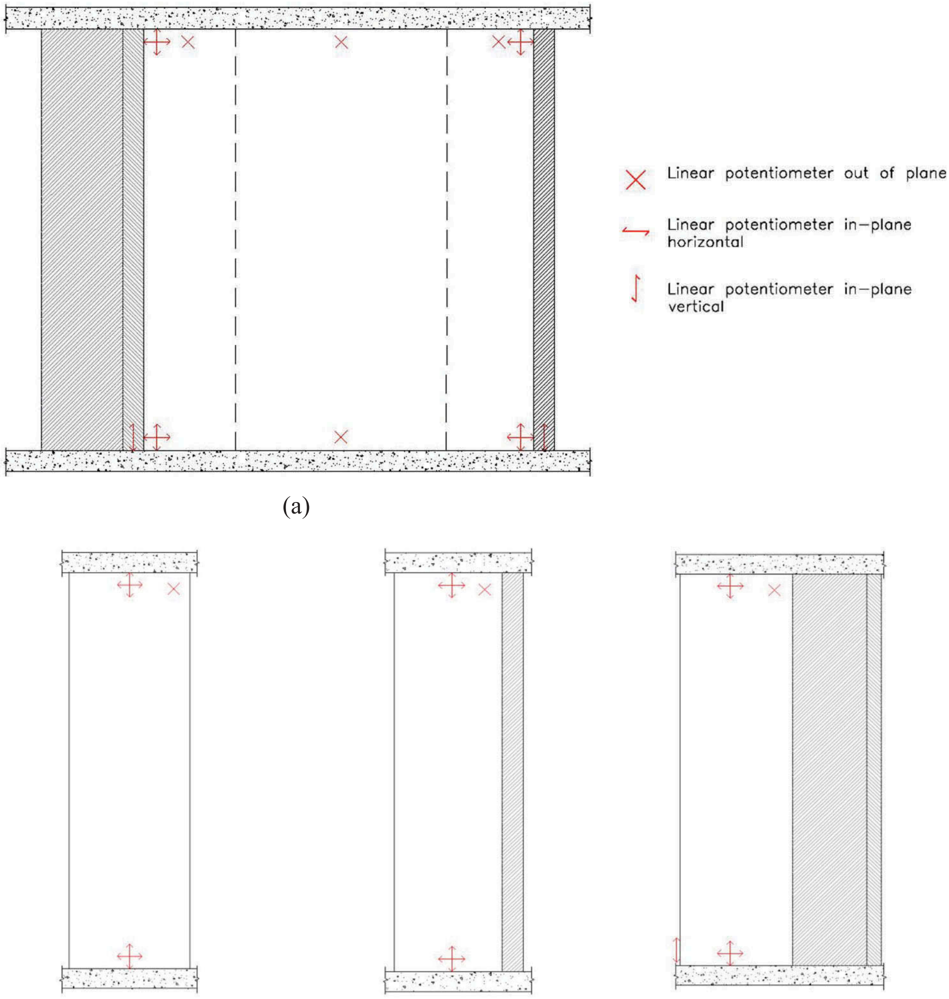

(a)

(b) (c) (d)

Figure 9. Typical potentiometer layout (a) primary wall north face (dotted lines show locations of lining interfaces) (b) west return wall east face (c) north east return wall west face (d) south east return wall east face.

damage observed during the tests are summarised in Table 1, along with their associated repair actions. Figure 10 illustrates the damage states being referred to in Table 1. These are similar to the conventional three damage states suggested by Taghavi and Miranda (2003), but include fire/acoustic sealant debonding as part of DS1. Note that typically failure of track anchors would be included within DS3, but as large anchors were used these did not damage in any case. Damage state 0 has been included to represent damage that is visible but is not considered to need repair depending on the required level of finish and a subjective assessment from the owner. The in-plane drift at which each damage state initiated in the specimens is shown in Table 2. Note that for DS3 the values recorded in Table 2 represent the final maximum drift the specimen was subject to before an inspection of the internal frame was

Table 1. Damage states.

Damage state	Description	Repair action
0	Hairline cracking of paint at joints	Barely visible damage, deemed not requiring repair.
1.a	Sealant de-bonding	Remove and re-apply sealant
1.b	Cracking in plaster and paint along trim	Scrape out minor cracks, and reapply plaster and paint.
1.c	Screw damage, pull through, popping, shearing	Refix or tighten any existing loose fasteners and place additional fasters near original. Finish with plaster, and sand and paint.
2	Wallboard damage – paper face separating, crushing, cracking, spalling	Requires replacement of linings or local repairs of linings. Breakages can be ground out and patch fixed, using plastering and paper tape.
3	Framing damage – flanges bent, buckling, hinging	Both linings and framing must be removed and replaced. Thus, complete demolition and replacement of the wall is required.

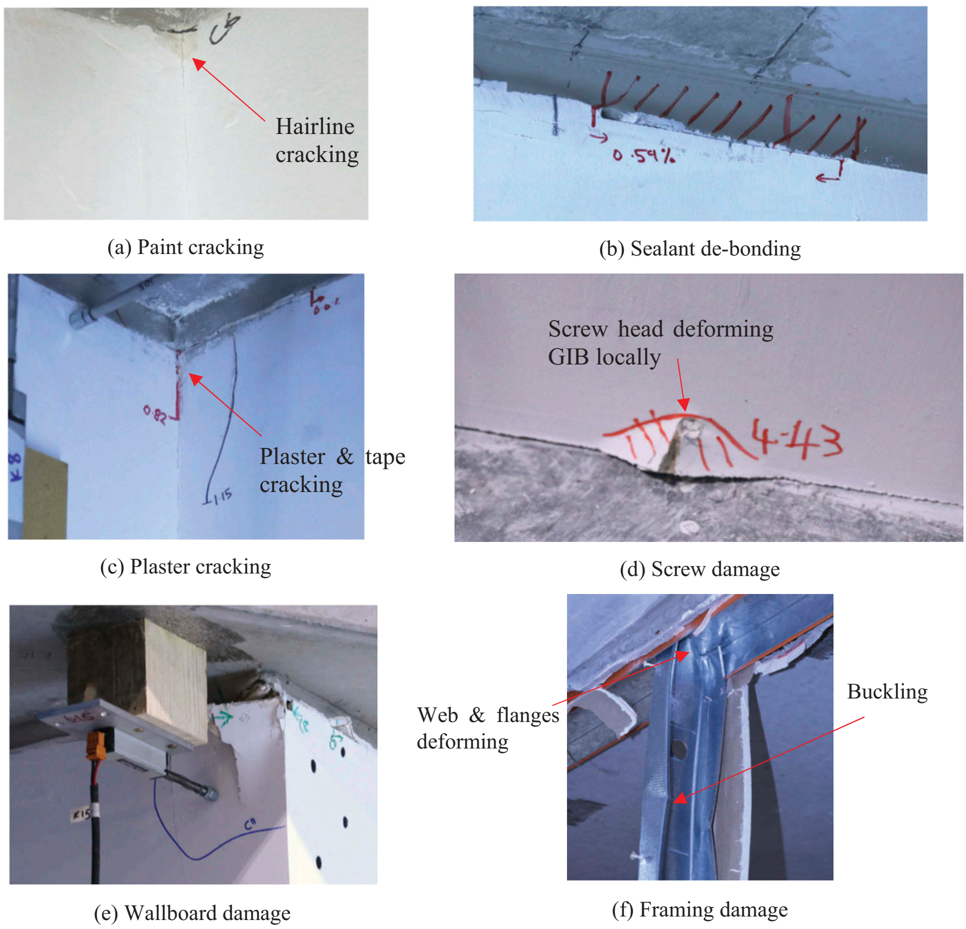

Figure 10. Examples of observed damage.

conducted. The formation of hinges in studs, associated with DS3, was discovered during the inspection performed following the tests, which indicates that the DS was triggered during testing at an unknown drift level. The formation of hinges in studs may be related to popping out screws around the hinge or strength degradation in the hysteresis loops. However, the

Table 2. In-plane drift %, r_i, at damage onset and fragility curve parameters.

	A1	A2	A3	x_m	β
DS1	0.36	0.26	0.26	0.29	0.35
DS2	0.36	0.26	0.26	0.29	0.35
DS3	<3.84	<3.84	<5.38	-	-

Table 3. Percentage of framing undamaged at the end of testing.

Test	Studs	Top tack	Bottom track
A1	46%	0%	100%
A2	39%	14%	100%
A3	24%	57%	57%

lowest drift level at which plasterboard panels need to be replaced corresponds to DS2 and as this type of repair work could reveal damaged studs, a lower-bound estimate for DS3 would be to adopt the same drift values as per DS2. The percentage undamaged framing at the end of the test is shown in Table 3. This value represents the length of undamaged framing at the end of the test as a percentage of the total original length of framing. Damage to the studs was more pronounced at the ends of walls and near the junctions; and damage to the steel tracks primarily occurred along the top, with more deformation near the junctions.

4.2. *Detailed Damage Progression*

The progression of damage in the specimens is detailed in Tables 4, 5, and 6. The drifts presented are the components of the total drift in-plane to the different wall orientations. The locations referred to in these tables are explained in Fig. 11. Each location refers to any vertical point of the wall within the region defined in Fig. 11. The damage states defined in Table 1 are used, and the entries in these tables represent the loading steps at which each damage state initiated at that location. For specimen A3, locations 4 and 13 refer to the section of wallboard above the doorway (lintel). For DS2, replacement of sealant and re-plastering is implied, therefore when DS2 occurs first or coincidentally with DS1, DS1 is not noted in Tables 4, 5, and 6.

4.3. *Behaviour Description & Discussion*

Damage was first observed as cracking of the wallboard at the wall end (location 21) for specimen A1, cracking of the wallboard at the junction (location 7) for specimen A2, and cracking of the wallboard propagating from the corners of the door opening (location 4 and 13) for specimen A3. The onset of DS1 and DS2 occurred simultaneously at a median in-plane drift of 0.29% and DS3 until the Linings had been removed at the end of the test (Table 2).

The mean damage state parameters and the damage progression was compared with similarly detailed specimens tested by Davies et al. (2011). Davies et al. (2011) tested two partially sliding specimens (specimen 34 and 36). Specimen 34 was detailed similarly to the specimens tested in this study: with track anchors removed only at the top, and linings fixed to the tracks at the bottom. In this specimen, damage was first observed with cracking of the joint tape at vertical wall junctions and popping out of screws connected

Table 4. Detailed damage progression for specimen A1 described in relation to damage states listed in Table 1.

	STEP	6	7	8	9	10	11	12	13	14	15
Drift (%)	Loading dir.	0.21	0.3	0.42	0.59	0.82	1.15	1.62	2.27	3.17	4.44
	45° wall	0.20	0.29	0.41	0.57	0.79	1.11	1.56	2.19	3.06	4.29
	90° walls	0.11	0.15	0.21	0.30	0.41	0.58	0.81	1.14	1.59	2.22
	Long wall	0.18	0.26	0.36	0.51	0.71	1.00	1.40	1.97	2.75	3.85
Location	**1**	-	-	-	-	-	-	-	1a,1c	-	2
	2	-	-	-	-	-	-	-	-	1a	-
	3	-	-	-	-	-	-	1a	1c	-	2
	4	-	-	-	-	-	1c	-	-	1a	2
	5	-	-	-	-	-	1c	-	-	1a	-
	6	-	-	-	-	-	-	-	1a,2	-	1b
	7	-	-	-	-	-	1a, 2		-	-	1c
	8	-	-	-	-	-	-	1a	-	-	-
	9	-	-	-	-	-	1a, 2	-	-	-	-
	10	-	-	-	-	-	-	1c	1a	-	1b
	11	0	-	1a,1b	-	-	-	-	2	-	-
	12	-	-	-	-	1a	-	-	1c,2	-	-
	13	-	-	-	-	-	-	-	1a	-	-
	14	-	-	-	-	-	-	-	1a	-	-
	15	-	0	1a	1b	-	-	-	-	-	2
	16	-	-	-	-	1a	-	-	-	2	-
	17	-	-	-	-	-	-	-	1a,2	-	1b
	18	-	-	-	-	1a	-	-		-	1b
	19	-	-	-	-	-	1b	-		1a	-
	20	-	-	-	-	-	-	-	1c	1a	-
	21	-	-	1a,2	-	-	-	-	-	1a	-

at the bottom track; and DS1, DS2, and DS3 initiated at 1.00%, 1.35%, and 1.84% drift, respectively. Therefore, damage progression of this specimen was significantly different from the specimens tested herein. This may be attributed to several factors including differing geometry; return wall configurations; junction details; the presence of a track anchor at the Y-junction; and bi-directional behaviour. The Davies et al. (2011) specimens were 3.5 m high and 3.7 m long, with 1.2 m returns at either end forming an I-shape configuration, whereas the specimens tested herein were 2.4 m high and 2.4 m long, with 0.6 m return walls in a y-shape. The junction details were significantly different. In the Davies et al. (2011) specimen there was no direct contact between the end of tracks and the linings. It is suspected that the factor providing the largest impact is this difference in detailing of the junctions.

The behaviour at the junctions was important. The first damage observed in specimen A2 was due to the top track pushing against the plasterboard lining and causing it to crack, thus initiating DS2, at a relatively low drift of 0.26%. The damage caused by the ends of track pushing against the lining was also the first damage seen in specimen A1, where the track pushed against the end of the return wall (location 20) at 0.36% drift. For specimen A3, the first observed damage was cracking of the linings at the corners of the doorway opening, however tracks pushing through linings did occur at larger drifts (0.71%). Cracking of linings from contact with track ends occurred at larger drifts for all specimens (locations 7, 8, 16, and 20). As this form of damage was seen consistently in all specimens, it is advised that future works could endeavour to solve this problem by

Table 5. Detailed damage progression for specimen A2 described in relation to damage states listed in Table 1.

	STEP	6	7	8	9	10	11	12	13	14	15
Drift (%)	Loading dir.	0.21	0.3	0.42	0.59	0.82	1.15	1.62	2.27	3.17	4.44
	45°	0.20	0.29	0.41	0.57	0.79	1.11	1.56	2.19	3.06	4.29
	90°	0.11	0.15	0.21	0.30	0.41	0.58	0.81	1.14	1.59	2.22
	Long wall	0.18	0.26	0.36	0.51	0.71	1.00	1.40	1.97	2.75	3.85
Location	**1**	-	-	-	-	-	-	-	1a	-	1b
	2	-	-	-	-	-	-	-	1a	-	1b
	3	-	-	-	-	-	-	1a	-	-	-
	4	-	-	-	-	-	-	1a	-	-	-
	5	-	-	-	-	-	1a	-	-	-	-
	6	-	-	-	-	-	2	-	-	-	-
	7	-	2	-	-	-	-	-	-	-	-
	8	-	-	-	-	-	1a	-	-	-	-
	9	-	-	-	-	1a	2	-		-	2
	10	-	-	-	-	-	1a	-	-	-	-
	11	-	-	-	-	0	-	-	-	1b	2
	12	-	-	-	1a	-	-	-	-	-	-
	13	-	-	-	-	-	-	-	1a	-	-
	14	-	-	-	-	-	-	-	1a	-	-
	15	-	0	-	-	-	1a,1b	2	-	-	-
	16	-	-	-	-	-	-	2	-	-	-
	17	-	-	-	-	-	-	2	-	-	-
	18	-	-	-	-	-	-	1a	-	2	1 c
	19	-	-	-	-	1a	0	-	-	1 c	1b,2
	20	-	-	-	-	-	-	1a	-	2	-
	21	-	-	-	2	-	-	-	-	-	-

either providing alternate junction details, or cutting the top tracks short of the ends of walls and junctions.

The effect of the door opening, in this system, was that instead of damage beginning at the ends of tracks (location 7 or 20), it began through diagonal cracking of the linings at the corners of the door opening on either side of the wall (location 4 and 12). This occurred at similar drifts to the onset of damage in specimens A1 and A2. Damage to other locations, including cracking of the linings, was delayed to higher drifts (0.71%). The 2D particle tracking shows that the doorway specimen behaved significantly different to the specimens without openings. Specimens A1 and A2 deformed very little in-plane, with minimal sliding and rocking, however, there was rocking due to out-of-plane displacements. For specimen A3, the plasterboard over the doorway cracked early on, and then either end of the wall (L- and Y-junction) moved as independent sections, with a greater degree of in-plane rocking and sliding. The difference between the behaviour of the specimens is shown in Fig. 12 and illustrated by the comparative sliding of the long wall in Fig. 13a, and the in-plane rocking of the 45° wall is shown in Fig. 13b.

It was intended to investigate the bi-directional behaviour by aligning the specimens at a 30° angle to the direction of loading (Fig. 5a). As no tests have been conducted on identical specimen's in-plane, a direct comparison cannot be made. However, the specimen detailing is similar to the Davies et al. (2011) specimen subgroup 1a commercial full-height slip track specimens, albeit with different return wall configurations. These specimens showed the onset of DS1 occurring at 0.26% in-plane drift, with no out-of-plane loading. And the median onset of damage for DS1 in this series of tests is 0.29% in-plane drift of the long wall and 0.17% out-of-plane drift along the long wall. Thus, it can be tentatively concluded that the out-of-plane

Table 6. Detailed damage progression for specimen A3 described in relation to damage states listed in Table 1.

	STEP	6	7	8	9	10	11	12	13	14	15	16
Drift (%)	Loading dir.	0.21	0.3	0.42	0.59	0.82	1.15	1.62	2.27	3.17	4.44	6.22
	45° wall	0.20	0.29	0.41	0.57	0.79	1.11	1.56	2.19	3.06	4.29	6.00
	90° walls	0.11	0.15	0.21	0.30	0.41	0.58	0.81	1.14	1.59	2.22	3.11
	Long wall	0.18	0.26	0.36	0.51	0.71	1.00	1.40	1.97	2.75	3.85	5.38
Location	**1**	-	-	-	-	-	-	-	-	1a	1c,2	1b
	2	-	-	-	-	-	-	-	-	1a	1b	2
	3	-	-	-	-	-	-	-	-	1a	1b,1c	2
	4	**0**	2	-	-	-	-	-	-	1a, 3*	-	3
	5	-	-	-	-	-	-	-	1a	-	-	-
	6	-	-	-	-	-	-	-	1a	-	1c,2	-
	7	-	-	-	-	-	-	-	1a	2	-	-
	8	-	-	-	-	-	-	-	-	1a,1c	-	-
	9	-	-	-	-	-	1a,2	-	-	-	-	-
	10	-	-	-	-	-	-	-	2	-	-	-
	11	-	-	-	0	1b	2	-	-	-	-	-
	12	-	-	-	-	-	-	-	1a	-	-	1c,2
	13	**0**	2	-	-	-	-	-	1a	-	-	-
	14	-	-	-	-	-	1a	-	-	-	-	1c,2
	15	-	-	-	0	1b	-	2	-	-	-	-
	16	-	-	-	-	-	1a	-	-	-	-	-
	17	-	-	-	-	-	-	1a	-	2	-	-
	18	-	-	-	-	-	1a	-	1b	2	1c	-
	19	-	-	-	-	-	-	-	1b	2	-	-
	20	-	-	-	-	-	1a	-	-	1b	2	-
	21	-	-	-	1b	2	-	-	-	-	-	-

3* refers to damage of the doorframe at which point the door could not be closed.

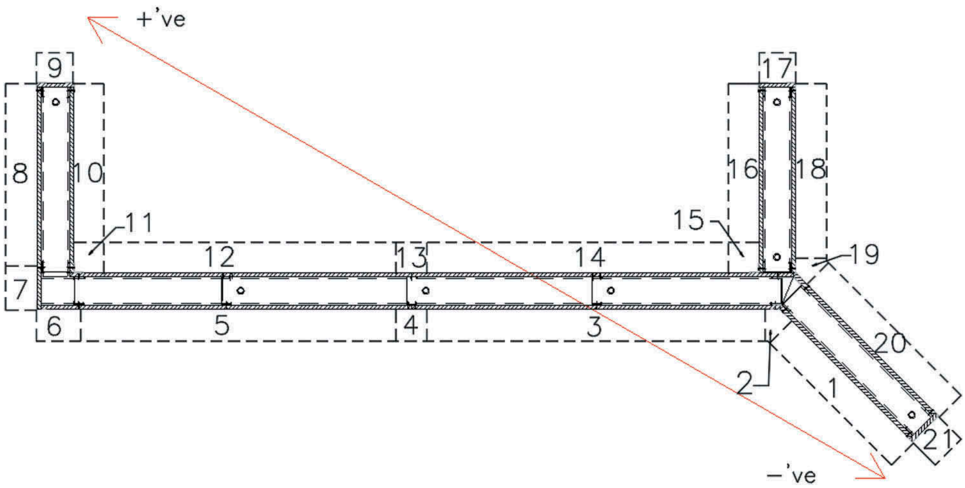

Figure 11. Specimen location reference for damage progression tables. Axis of loading a definition of positive loading direction shown in red.

demand did not significantly impact the fragility. Additionally, by comparing the drift at which the ends of the return walls damaged in each specimen (Table 7), it can be seen that for locations 9 and 21, this occurred at a similar level of in-plane displacement, even though the

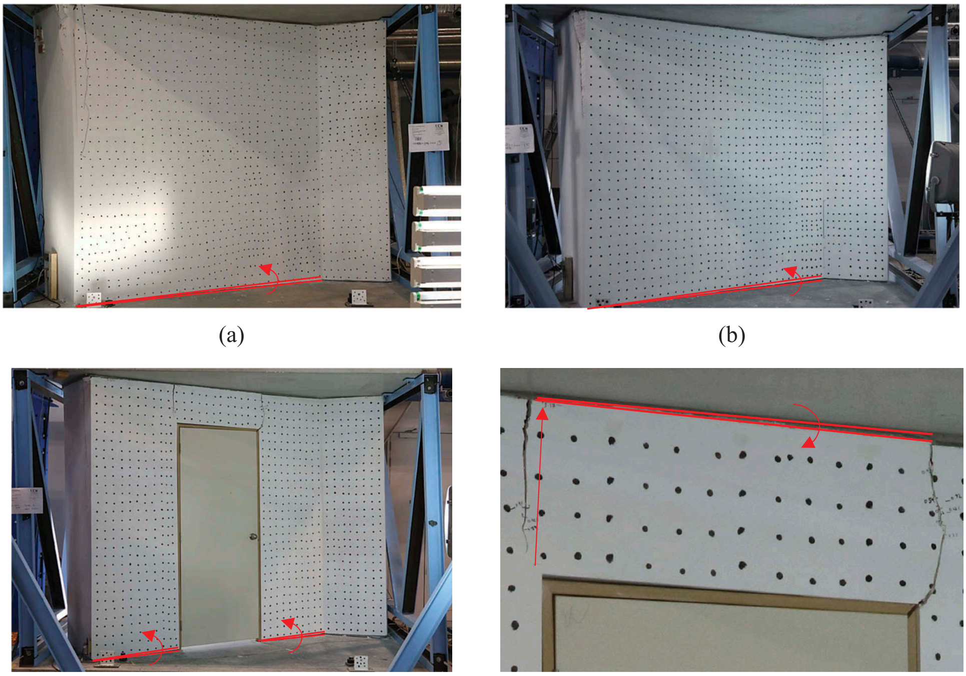

(a) (b) (c) (d)

Figure 12. Visual comparison of the behaviour of specimens at the first peak of loading step 15 (4.44% drift): (a) specimen A1, (b) specimen A2, (c) specimen A3, and (d) specimen A3 showing sealant deformation above doorway.

walls were at a different angle to the applied loading. This suggests that this form of damage is best correlated to the in-plane displacement of the wall.

Location 17 appeared to perform better in terms of wallboard damage (Table 7), which is suspected to be due to the unique Y-shape at the junction and the position of the top track anchors. As the top track anchors are removed from the long wall and the 45° angled wall close to the junction, the track is flexible out-of-plane at these location. When the specimen is pushed in the positive direction (as defined in Fig. 11), the top track in the 90° wall pushes at the end (location 17) and the 45° wall will push against the linings (between locations 15 & 19). As the 90° wall is being forced in the positive direction by both the track in the 45° wall and the track in the 90° wall the linings tend to slide and rotate in the direction of loading instead of cracking at location 17. The asymmetric behaviour at the Y-junction is illustrated in Fig. 14, which shows the relative out-of-plane displacement between the lining and the top slab at the corners of the long wall (location 15/Y-junction). When the wall is pushed in the positive direction, if the long wall is to remain in position, there will be a positive relative out-of-plane displacement reading and vice versa. If the wall moves with the imposed displacement the value of out-of-plane displacement will be zero. This figure shows that the amplitude of the excursions is greater when the wall is pushed in the positive direction demonstrating that the top track is flexing, but when loaded in the negative direction, the top track in the long wall is unable to flex giving smaller amplitude readings. As a result, the 90° return slides prefer-

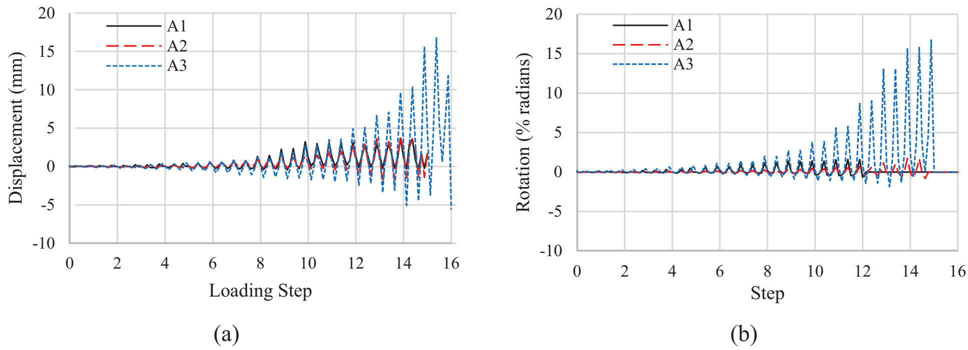

Figure 13. Comparison of behaviour of partition specimens. (a) long-wall in-plane sliding and (b) rotation of 45° return wall (*data missing for specimen A1 due to instrumentation failure).

Table 7. Summary of wallboard damage progression at wall ends.

	DS2: Wallboard damage					
	Dir. Of	Location	A1	A2	A3	Mean
In-plane drift (%)	90° wall	9	0.58	0.58	0.58	0.58
	90° wall	17	1.14	0.81	1.59	1.18
	45° wall	21	0.41	0.57	0.79	0.59

entially when loaded in the positive direction to the negative, which is supported by Fig. 15a and b; the long wall slides preferentially in the positive to the negative direction; and the 45° wall rotates when loaded in the positive direction more than the negative (Fig. 13).

The out-of-plane behaviour at the Y-junction can be contrasted to the out-of-plane relative movement measured at the L-junction (Fig. 14, shown in red). The movement at the L-junction showed preference to negative displacement for specimen A1 and A2, although specimen A2 was approximately symmetrical for the initial cycles. The data for specimen A3 was lost due to issues with the potentiometer during testing. The preference to negative displacement is attributed to how when loaded in the positive direction the top track of the 90° wall pushes through the end and thus the wall movement is only forced by the top track of the long wall, thus there is larger out-of-plane displacement measured as the wall attempts to remain stationary while the top slab moves. When loaded in the negative direction, the top track of the 90° return pushes against the top track of the long wall such that the wall is forced by both the movement of the 90° return top track and the long-wall top track, and there is very little relative displacement between the top slab and the out-of-plane potentiometer.

The effect of the angled return wall has been discussed above. It can also be seen that the junction between the 45° return wall and the main wall or 90° return wall experienced very little damage (location 2 and 19). DS1 initiated in this junction at 1%, 2.75%, and 1.96% drift for specimen A1, A2, and A3, respectively. The resistance to damage at this junction may be attributed to the rigidity of the joint itself. The joint was reinforced with 0.55 bmt galvanised 135° steel angles screwed to the studs at this location, so this may have reduced the differential movement between the wall panels. Figure 16c shows that the top track from

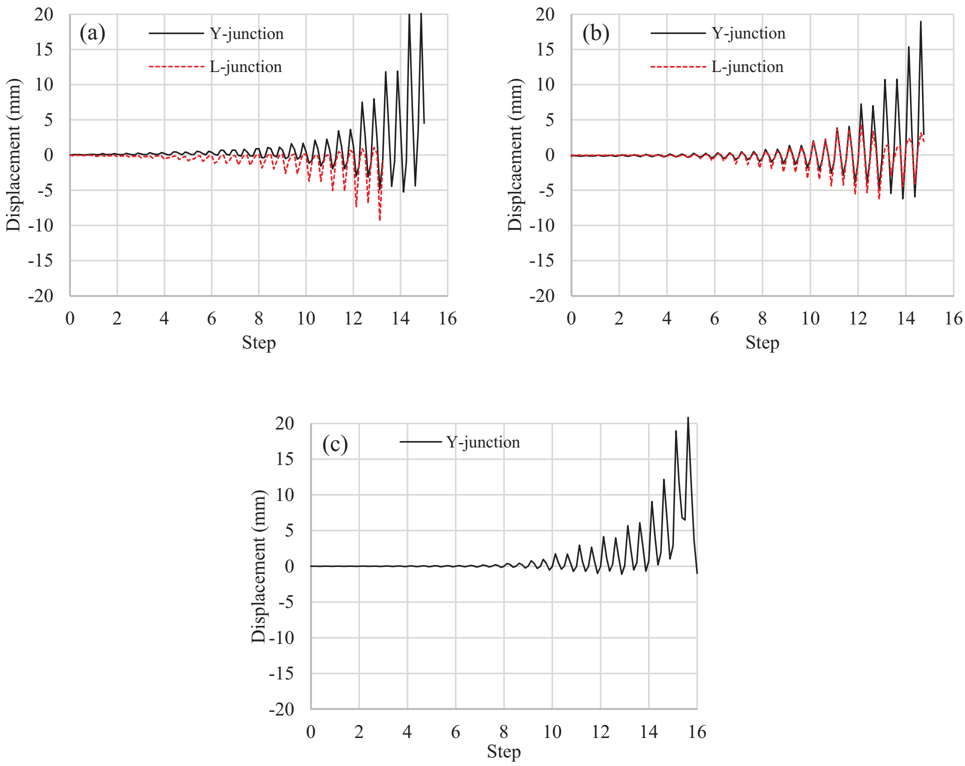

Figure 14. Out-of-plane relative displacement at the top of the long-wall corners at the Y- and L-junctions for specimen (a) A1 (*data missing due to instrumentation failure) (b) A2, and (c) A3 (*data missing for L-junction due to instrumentation failure).

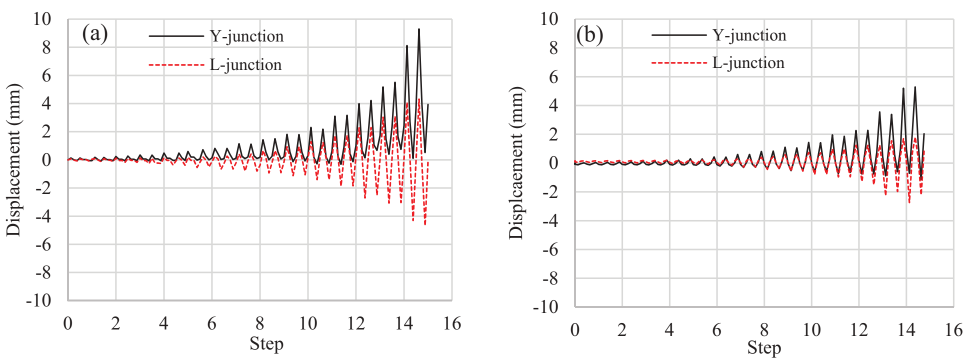

Figure 15. In-plane sliding of 90° return walls for specimens (a) A1 and (b) A2.

the long wall and the 45° wall at the Y-junction have pushed hard up against the 90° wall top track at the end of the test. This represents the residual displacement of the joint after a negative loading peak excursion of 150 mm displacement or 6.2% drift. This shows how when loaded in the negative direction the top track of the 90° return wall pushes against the junction, which is attempting to remain stationary as the track anchors at this location are removed. The bending of the flanges at this location is attributed to the fact that the end studs are rigidly attached to the junction and therefore the linings are attempting to remain stationary, while the top track is forced by the anchor at this location to move. It is noted that if the anchor had been removed, this form of damage may have been avoided, and consequently damage at locations 15 and 19 reduced. The relative out-of-plane displacement between the 90° wall and the top slab, measured near location 19 is shown in Fig. 16d.

No damage was observed along the field of the wall due to the out-of-plane displacements (other than to sealant). This is because the wall is relatively flexible out-of-plane. The influence of bi-directional behaviour becomes important at the junctions between neighbouring walls. The results showed that the behaviour of the wall specimens depends on the direction of loading. The results from the test on specimen A3 suggest that the walls deform as a unit rather than as separate walls. Therefore, bi-directional behaviour is deemed significant, even if its impact cannot be quantified by this test.

The sealant was applied over a 25 mm gap at the top of the linings on all specimens. Sealant damaged at 0.36% (locations 10 and 20), 0.51% (locations 11 and 20), and 0.71% (location 10) in-plane drift for specimens A1, A2, and A3, respectively. The damage at locations 20 (the end of the angled return wall) was coincident with the cracking of the linings, whereas for location 10 the damage was in the sealant bond itself. The damage to the sealant first occurred around

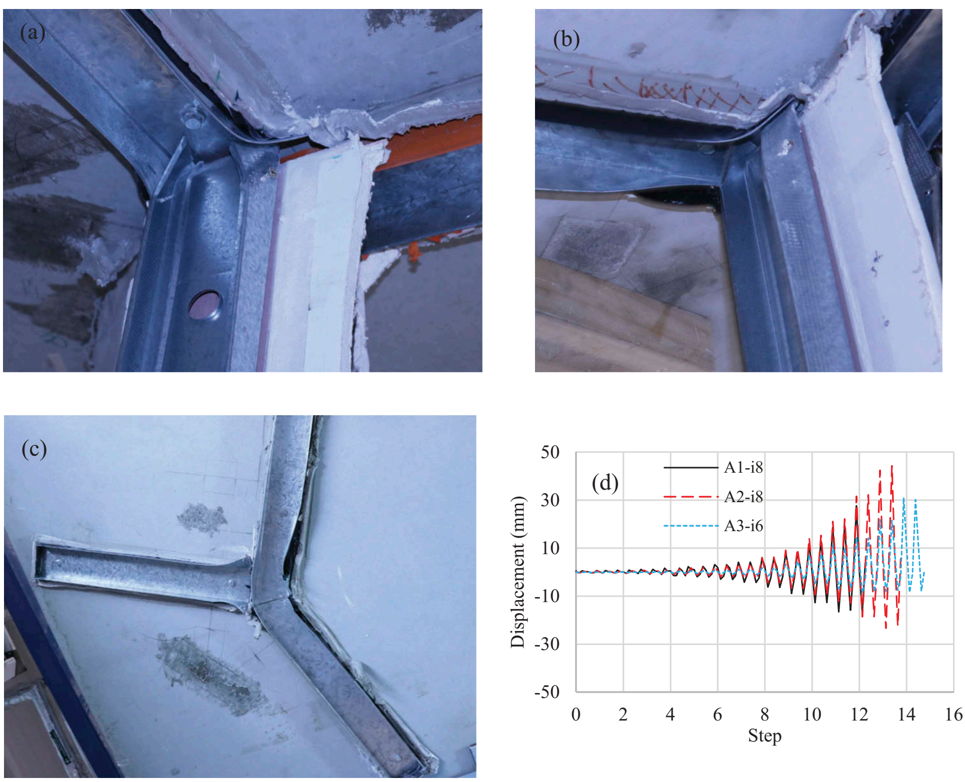

Figure 16. Damage to steel tracks at Y-junction for specimen (a) A1 (b) A2, and (c) A3. In particular, showing bent flanges of 90° angled wall top track. (d) Shows the out-of-plane relative movement between 90° return wall at location 19 top corner and top slab for the three specimens (*data missing for specimen A1 due to instrumentation failure).

areas of high deformability (i.e. at the junctions) at drifts greater than 0.36%, whereas damage to sealant away from junctions typically occurred at higher drifts (0.7–1%) irrespective of whether this was in the primary length of the wall or in a return wall (i.e. in-plane or out-of-plane demand). Damage consisted primarily of separation at the lining interface initially, but for some parts of the wall, at higher drifts, the sealant remained bonded and ruptured in the middle of its depth. This suggests that the bond between the plasterboard and the sealant is very important for the seismic performance, as if the sealant is well-bonded, it can sustain higher demands. It was also noted that after the sealant had cured there was a significant number of defects in the bond to the plasterboard. Therefore, it is advised that careful quality control is maintained when applying similar products, as defects in the bond may hamper the effectiveness of their fire and acoustic performance, and reduce ability to withstand seismic movement.

4.4. *Fragility*

The most common form of a seismic fragility function is the lognormal cumulative distribution function (CDF):

$$F_d(x) = P[D \geq d|X = x], \quad d \in \{1, 2, \ldots, Nd\}$$

$$\Phi = \left(\frac{\ln(x/\theta_d)}{\beta_d}\right) \tag{1}$$

The experimental results from the test were used to produce a set of fragility curves for the damage states defined in Table 1. The three specimens were grouped together to represent the seismic fragility of a partition specimen with an arbitrary configuration (Fig. 17) and compared with fragility subgroup 1a from the Davies et al. (2011) tests. These specimens have similar detailing to the typical NZ partition wall. The in-plane displacement of the primary section of the wall was used as the engineering design parameter (EDP) to correlate between damage and demand, according to Porter, Kennedy, and Bachman (2007). The framework proposed by Porter, Kennedy, and Bachman (2007) for experimentally determined fragility curves, Method A, was used (Equations 1 & 2), where M is the number of specimens tested to failure; i is the index of the specimens,$i \in \{1, 2, \ldots, M\}$; ri is the EDP at which damage was observed to occur in specimen i; x_m is the median; β is the random logarithmic standard deviation; and as less than five specimens were tested and the specimens were loaded according to the same protocol, an additional term β_u was introduced according to the guidelines in Porter (2018) and FEMA (2012). This additional term represents uncertainty that the tests represent actual conditions of installation and loading, or uncertainty that the available data are an adequate sample size to accurately represent the true random variable. The fragility parameters for each damage state are shown in Table 2.

$$x_m = exp\left(\frac{1}{M}\sum_{i=1}^{M} lnr_i\right) \tag{2}$$

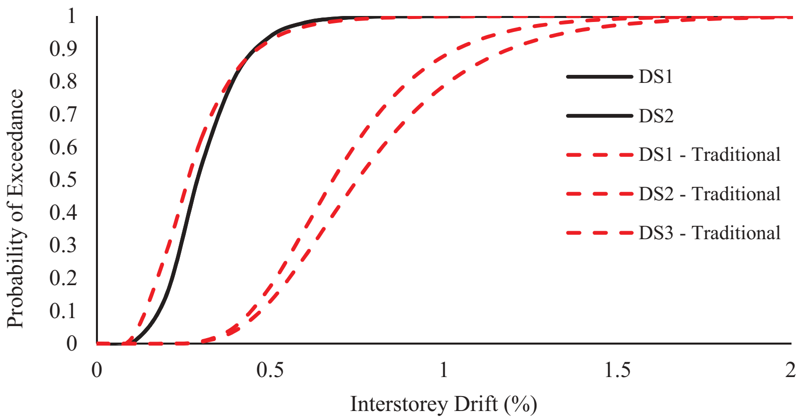

Figure 17. Seismic fragility curves superimposed with Davies et al. (2011) fragilities for subgroup 1a – full-height commercial slip tracks (red).

$$\beta = \sqrt{\frac{1}{M-1}\left(\sum_{i=1}^{M}\left(\ln\left(\frac{ri}{x_m}\right)\right)^2\right)} \tag{3}$$

$$\beta' = \sqrt{\beta^2 + \beta_u^2} \tag{4}$$

The fragility parameters that result from this experiment are not necessarily directly relatable to previous tests. This is because the damage states do not imply the same loss functions. A loss function represents the probable loss associated with a component in the event of an earthquake for each damage state of the component. The repair costs of partitions have been calculated previously, as in Taghavi and Miranda (2003). These estimates are based on the three distinct repair actions: (1) tape and finish and paint with roller on both sides; (2) remove damaged boards on both sides, replace boards, tape and finish, and paint with roller on both sides; and (3) remove damage boards, remove damaged metal frames, replace framing, replace gypsum boards on both sides, tape and finish, and paint with roller on both sides. The estimates for repair cost are made assuming that finishing, replacement of gypsum board, and replacement of framing is required at every location. In particular, for this series of experiments, the wallboard damage was highly localised, and the point at which DS2 has been reported to initiate does not imply the wallboard in every location requires replacement. Therefore, if a loss assessment was conducted using conventional loss functions, it is expected that they would overestimate losses.

4.5. *Force-Displacement Behaviour*

The first two specimens, A1 and A2, were identical, but their hysteretic responses were significantly different. It can also be seen that the damage progression in A1 was significantly different from A2 (Tables 4 and 5). The capping forces the two loading directions varied in both specimens, but no significant bias can be seen in either direction. The average capping force in the positive and negative directions for the three specimens are 9.83 kN at 2.2% and 9.79 kN at 2.19%, respectively (Table 8). The difference in behaviour may be attributed to a number of factors including variations in material properties and construction quality.

4.6. Energy Absorption

The equivalent viscous damping was determined at each cycle according to Equation 5 (Calvi, Priestley, and Kowalsky 2007), and is shown in Fig. 19b. Where A_h is the energy absorbed during a complete cycle, F_m is the maximum force experienced in the cycle, and Δ_m is the maximum displacement experienced in the cycle. The energy absorbed by the specimen is defined as the area under the force-displacement curve. The hysteretic curves shown in Fig. 18 were integrated using the trapezium method for each increment in data. The energy dissipated in the two cycles of loading at each amplitude were averaged to attain the average energy dissipation at each step (Fig. 19a).

$$\xi_{hyst} = \frac{A_h}{2\pi F_m \Delta_m} \tag{5}$$

The data is not available for the small cycles of specimen A1, as there were some issues with the loading and instrumentation setup-early on in the testing. Therefore, the calculation of energy dissipation during these early cycles is uncertain. Data is shown for loading cycles 11 to 15, which corresponds to 1.15% to 4.44% drift in the direction of loading.

4.7. Numerical Model Calibration

For numerical investigation purposes, the experimental results were used to calibrate a hysteretic model. Because of the significance of pinching, the hysteresis rule used to describe the behaviour of the partition specimens was the Wayne–Stewart degrading stiffness model (Fig. 20) available in Ruaumoko 2D (Carr 2008). The key parameters of the model are described in Table 9.

The first step in calibrating the Wayne–Stewart hysteretic model is to determine the backbone curves from the experimental data. The backbone curves were generated by tracking the force associated with the maximum displacement excursions. The idealized force-displacement backbone curve is characterized by eight points, four positive and four negative. The selection of these points is guided by calculating the first derivative of the backbone curve (tangent stiffness). The tri-linear factor beyond the ultimate force is taken as zero for all specimens and the strength degradation was modelled as dependent on ductility. The parameters were then calibrated to each specimen depending on the shape of the curves and the relative energy dissipation between the analytical and experimental results. The final calibrated model factors are

Table 8. Ultimate loads.

Specimen	−ve Max load (kN)	−ve Drift (%)	+ve Max load (kN)	+ve Drift (%)
A1	7.59	2.09	9.58	2.14
A2	10.57	2.25	10.37	2.27
A3	11.20	2.25	9.53	2.17

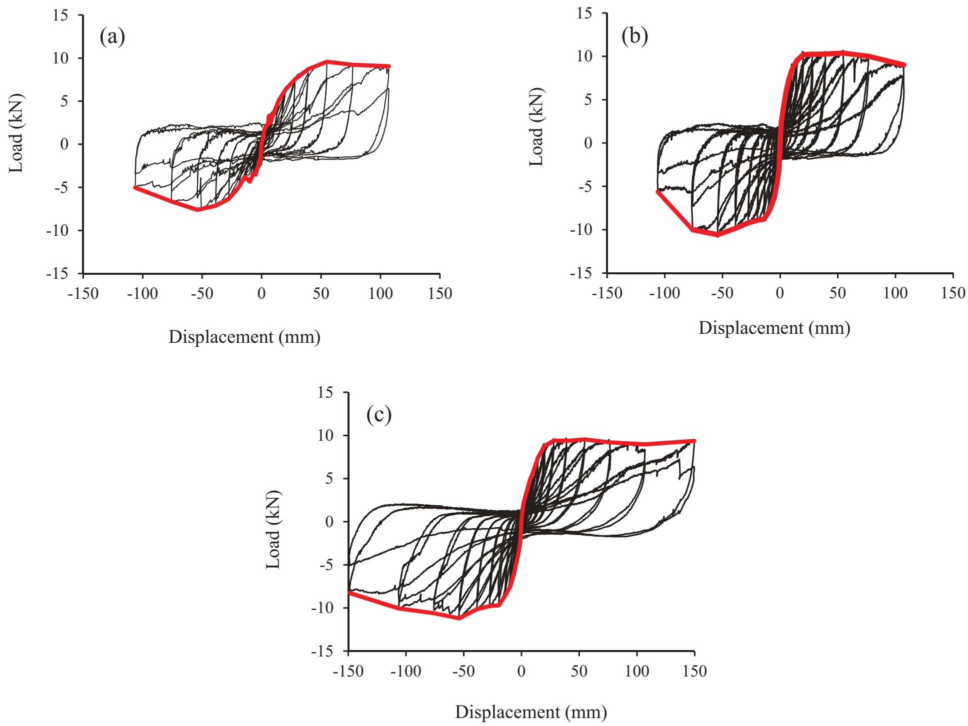

Figure 18. Hysteresis results and backbone curves for (a) Specimen 1, (b) Specimen 2, and (c) Specimen 3.

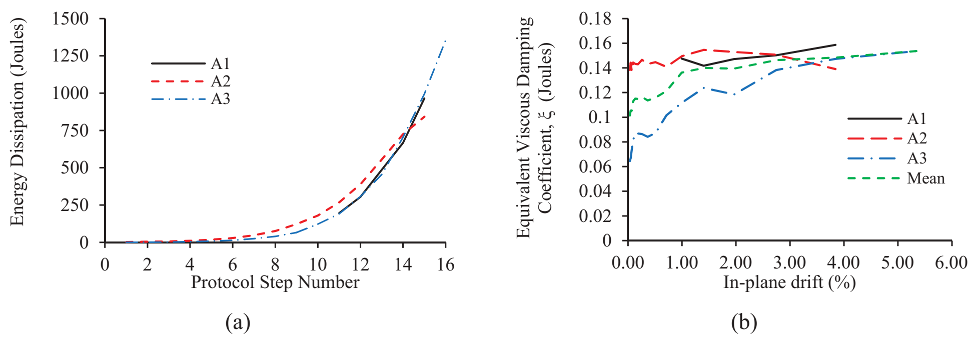

Figure 19. (a) Energy dissipation during each step; (b) Equivalent viscous damping coefficient for each cycle versus in-plane drift demand.

shown in Table 9, and the corresponding analytical hysteretic curves are plotted against the experimental results in Fig. 21. A final model representing the mean behaviour across the specimens is illustrated in Fig. 21d.

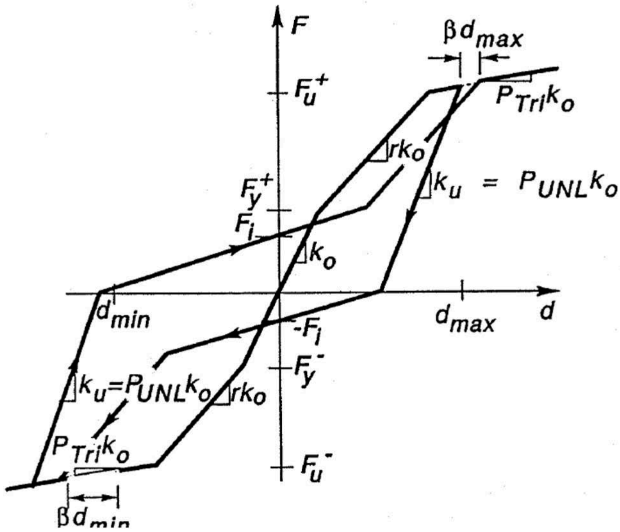

Figure 20. Wayne–Stewart Degrading Hysteresis model available in Ruaumoko 2D (Carr 2008).

Table 9. Calibrated Wayne–Stewart Hysteretic model parameters for each specimen.

Key parameters		Specimen 1	Specimen 2	Specimen 3	Mean
Ko	Stiffness	0.83	1.37	1.10	1.10
PTRI	Tri-linear factor beyond ultimate force or moment	0.00	0.00	0.00	0.00
FU+	Positive ultimate force	9.58	10.37	9.53	9.83
FU-	Negative ultimate force	−7.59	−10.57	−11.20	−9.79
M1	Ductility at start of degradation	1.74	4.67	2.54	2.98
M2	Ductility at finish of degradation	2.84	6.27	5.79	4.97
M3	Final fraction of strength	0.80	0.68	0.86	0.78
M4	Ductility at 1% of initial strength	-	-	-	-
FY	Yield force or moment (>0):	3.03	5.08	5.57	4.56
FI	Intercept force or moment (>0):	1.50	1.50	1.50	1.50
R	Bi-linear factor (<0.9) or Ramberg-Osgood Factor (>1)	0.25	0.32	0.23	0.26
PUNL	Unloading stiffness factor (>1):	1.50	1.50	1.50	1.50
GAP+	Initial slackness in positive axis,Diagonal gap (>0):	0.00	0.00	0.00	0.00
GAP-	Initial slackness in negative axis, Diagonal gap (<0):	0.00	0.00	0.00	0.00
BETA	Softening factor (≥1):	1.03	1.08	1.03	1.05
ALPHA	Pinch power factor (≤1):	0.55	0.60	0.55	0.57
IOP	0 for the unmodified loop, 1 for the modified loop:	1.00	1.00	1.00	1.00

Factors M1 to M4 are parameters corresponding to strength degradation type 1, where strength degradation depends on the ductility.

5. Conclusions

Three specimens with partly sliding detailing, consisting of top tracks that are not bolted at intersections, were subjected to quasi-static cyclic testing. The specimens were aligned at 30° and the y-shaped configuration meant bi-directional behaviour could be examined. The specimens included an acoustic/fire sealant. Although the top track anchors were specified to be removed within 600 mm of wall intersections, a construction error was made whereby a single top track slab to concrete anchor was left in at the three-way wall junction (Fig. 4). Despite this error, the experimental testing was deemed worthwhile since

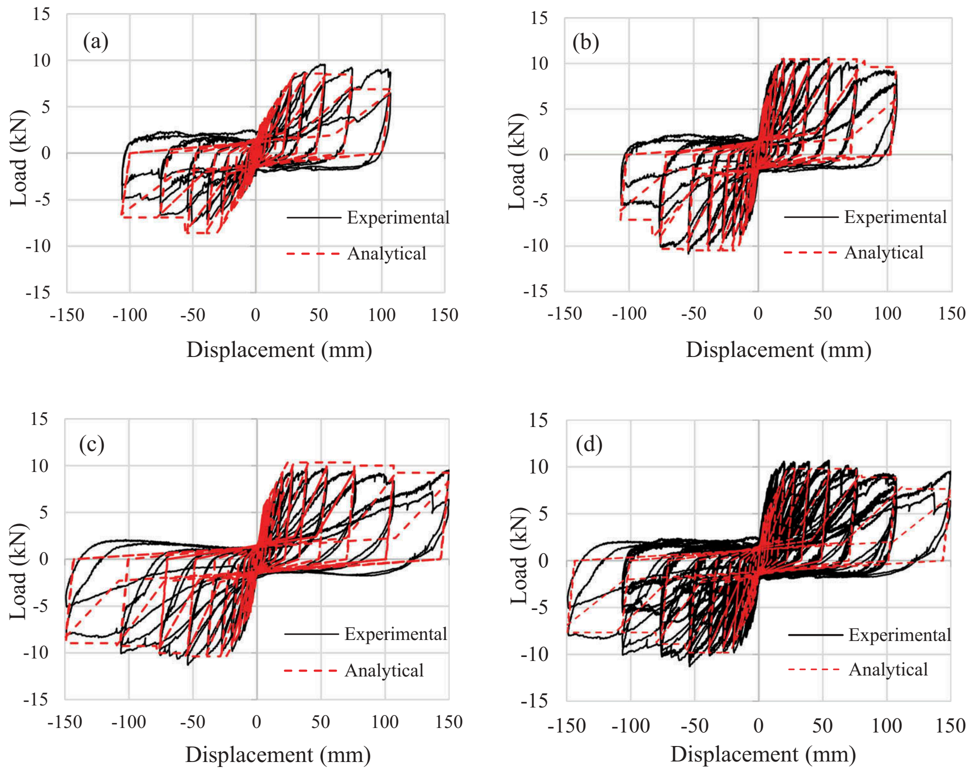

Figure 21. Wayne–Stewart hysteretic model fit of experimental hysteresis; (a) Specimen A1, (b) Specimen A2, (c) Specimen A3, (d) All specimens with mean parameter model fit.

such errors will also occur in practice and because the behaviour of the wall can be examined with this fixing in mind.

In addition to providing drift capacities, the force-displacement behaviour has been reported, energy dissipation computed, and parameters of the Wayne–Stewart hysteretic model fitted to the test results. This information may be useful for those interested in undertaking refined analyses of partition walls.

The main findings from this experimental programme are summarised as follows:

- Damage was first observed as cracking of the wallboard at the wall ends, at external junctions, and propagating from the corners of the door opening. The onset of DS1 and DS2 occurred simultaneously at a median in-plane drift of 0.29% and damage state DS3 was not observed until after the linings had been removed at the end of the test, which indicates that the DS was triggered during the testing at an unknown drift level.
- The specimen with the door opening (specimen A3) behaved differently to the plane specimens (specimens A1 & A2). Damage began as cracking of the wallboard propagating from the corners of the doorway, at similar drift levels to specimens A1 and A2. Following the separation of the wallboard above the lintel, the L- and Y-junctions behaved as independent wall sections, and damage elsewhere was delayed.

- No damage was observed along the field of the wall due to out-of-plane displacements (other than to sealant). This is because the wall is relatively flexible out-of-plane. The results showed that the behaviour of the wall specimens depends on the direction of loading and that the walls deform as a unit rather than separately. Therefore, bi-directional behaviour is deemed significant, even if its impact cannot be directly quantified by this test.
- Damage to sealant first occurred around areas of high deformability (i.e. at the junctions) at drifts greater than 0.36%. Whereas damage to sealant away from junctions typically occurred at higher drifts (0.7–1%) irrespective of whether this was in the primary length of the wall or in a return wall (i.e. in-plane or out-of-plane demand). Results suggest that the bond between plasterboard and sealant is important for the seismic performance. It was also noted that after the sealant had cured there was a significant number of defects in the bond to the plasterboard. Therefore, it is advised that careful quality control is maintained when applying similar products, as defects in the bond may hamper the effectiveness of their fire and acoustic performance, and reduce ability to withstand seismic movement.

Acknowledgements

The authors gratefully acknowledge the funding support offered by The International Collaborative Research program of the Disaster Prevention Research Institute, Kyoto University under Project Number 28W-03 (PI: Timothy Sullivan), the NZ Property Council, and Quake Centre. This project was also partially supported by QuakeCoRE, a New Zealand Tertiary Education Commission-funded Centre. This is QuakeCoRE publication number 0457′. Thanks also to the industry partners; RONDO; Winston Wallboards; Dunning Thornton Consultants; and Holmes Consulting.

Funding

This project was partially supported by QuakeCoRE, a New Zealand Tertiary Education Commission-funded Centre. This is QuakeCoRE publication number 0560.

ORCID

T. J. Sullivan http://orcid.org/0000-0002-6997-5434
R. P. Dhakal http://orcid.org/0000-0001-5524-5919

References

Araya-Letelier, G., and E. Miranda. 2012. Novel sliding/frictional connections for improved seismic performance of Gypsum Wallboard partitions. 15th World Conference on Earthquake Engineering. doi:10.1094/PDIS-11-11-0999-PDN.

Arifin, F. A., T. J. Sullivan, and G. A. Macrae. 2017. *Identification of cost-effective retrofit and/or rehabilitation strategies for steel buildings*. Christchurch, New Zealand: University of Canterbury.

Calvi, G. M., M. J. N. Priestley, and M. J. Kowalsky. 2007. *Displacement-based seismic design of structures*. Pavia, Italy: IUSS PRESS.

Carr, A. 2008. *Ruaumoko manual - volume 5: Appendices*. Christchurch, New Zealand: Department of Civil Engineering, University of Canterbury. doi:10.13140/RG.2.1.4493.7127.

Davies, R. D., R. Retamales, G. Mosqueda, and A. Filiatrault. 2011. *Experimental seismic evaluation, model parameterization, and effects of cold-formed steel-framed gypsum partition walls on the seismic performance of an essential facility*. Multidisciplinary Center forEarthquake Engineering Research Rep. MCEER-2011-05. Buffalo, NY: University at Buffalo, State University of New York.
Deierlein, G. G., H. Krawinkler, and C. Allin Cornell. 2003. A framework for performance-based earthquake engineering. In 2003 Pacific Conference on Earthquake Engineering, vol. 273, 140–48. Christchurch, New Zealand. doi:10.1061/9780784412121.173.
Dhakal, R. P. 2010. Damage to non-structural components and contents in 2010 darfield earthquake. *Bulletin of the New Zealand Society for Earthquake Engineering* 43 (4): 404–10. doi: 10.5459/bnzsee.43.4.404-411.
FEMA, Federal Emergency Management Agency. 2007. Interim testing protocols for determining the seismic performance characteristics of structural and nonstructural components. FEMA 461, Washington, DC: FEMA. https://www.fema.gov/media-library/assets/documents/15207.
FEMA, Federal Emergency Management Agency. 2012. *Seismic performance assessment of buildings*. Fema P-58. vols. 1–7. Washington, DC: FEMA.
Freeman, S. A. 1971. Third progress report on racking tests of wall panels. JAB-99-54, Berkeley: University of California.
GIB. 2012. *GIB fire rated systems*. Auckland, New Zealand: Winstone Wallboards.
Krawinkler, H., F. Parisi, L. Ibarra, A. Ayoub, and R. Medina. 2001. Development of a testing protocol for woodframe structures. CUREE - Caltech Woodframe Project. Richmond, California, 1–76. https://www.curee.org/publications/woodframe/downloads.
Lee, T. H., M. Kato, T. Matsumiya, K. Suita, and M. Nakashima. 2007. Seismic performance evaluation of non-structural components: Drywall partitions. *Earthquake Engineering & Structural Dynamics* 36 (3): 367–82. doi: 10.1002/eqe.638.
Magliulo, G., C. Petrone, V. Capozzi, G. Maddaloni, P. Lopez, and G. Manfredi. 2014. Seismic performance evaluation of plasterboard partitions via shake table tests. *Bulletin of Earthquake Engineering* 12 (4): 1657–77. doi: 10.1007/s10518-013-9567-8.
Pali, T., B. Bucciero, M. T. Terracciano, V. Macillo, L. Fiorino, and R. Landolfo. 2017. In-plane quasi-static cyclic tests on lightweight steel drywall non-structural partition walls. *Eurosteel* 1: 2857–66. Copenhagen, Denmark. doi:10.1002/cepa.337.
Pali, T., V. Macillo, M. Terracciano, B. Bucciero, L. Fiorino, and R. Landolfo. 2018. In-plane quasi-static cyclic tests of nonstructural lightweight steel drywall partitions for seismic performance evaluation. *Earthquake Engineering & Structural Dynamics* 47: 1566–88. doi: 10.1002/eqe.3031.
Porter, K. 2018. *A Beginner's guide to fragility, vulnerability, and risk*. Denver, CO. doi:10.1007/978-0-387-93837-0.
Porter, K., R. Kennedy, and R. Bachman. 2007. Creating fragility functions for performance-based earthquake engineering. *Earthquake Spectra* 23 (2): 471–89. doi: 10.1193/1.2720892.
Restrepo, J. I., and A. M. Bersofsky. 2011. Performance characteristics of light gage steel stud partition walls. *Thin-Walled Structures* 49 (2): 317–24. doi: 10.1016/j.tws.2010.10.001.
Retamales, R., R. Davies, G. Mosqueda, and A. Filiatrault. 2013. Experimental seismic fragility of cold-formed steel framed gypsum partition walls. *Journal of Structural Engineering* 139 (8): 1285–93. doi: 10.1061/(ASCE)ST.1943-541X.0000657.
Rihal, S. S. 1980. *Final technical report racking building tests of non-structural partitions. The behavior of architectural (non-structural) building components during earthquakes*. San Luis Obispo, CA: California Polytechnic State University.
Taghavi, S., and E. Miranda. 2003. Response assessment of nonstructural building elements. Report 2003/05, University of California Berkeley.
Tasligedik, A. S., S. Pampanin, and A. Palermo. 2015. Low damage seismic solutions for non-structural drywall partitions. *Bulletin of Earthquake Engineering* 13 (4): 1029–50. doi: 10.1007/s10518-014-9654-5.
Whitman, R. V., S.-T. Hong, and J. W. Reed. 1973. *Damage statistics for highrise buildings in the vicinity of the San Fernando earthquake. Structures publication No. 363*. Cambridge: M.I.T., Dept. of Civil Engineering.